Received: 19 October 2022 | Revised: 30 March 2023 | Accepted: 27 May 2023

DOI: 10.1002/aic.18189

AIChE JOURNAL

RESEARCH ARTICLE

Thermodynamics and Molecular-Scale Phenomena

Charging dynamics in a laminate-electrode model for graphene-based supercapacitors

Haolan Tao [1,2] | Zhi Xu [1] | Cheng Lian [1] | René van Roij [2] | Honglai Liu [1]

[1]State Key Laboratory of Chemical Engineering, School of Chemical Engineering, East China University of Science and Technology, Shanghai, China

[2]Institute for Theoretical Physics, Center for Extreme Matter and Emergent Phenomena, Utrecht University, Utrecht, The Netherlands

Correspondence

Zhi Xu, State Key Laboratory of Chemical Engineering, School of Chemical Engineering, East China University of Science and Technology, Shanghai 200237, China.
Email: zhixu@ecust.edu.cn

Cheng Lian, State Key Laboratory of Chemical Engineering, School of Chemical Engineering, East China University of Science and Technology, Shanghai 200237, China.
Email: liancheng@ecust.edu.cn

Funding information

EU-FET project NANOPHLOW, Grant/Award Number: REP-766972-1; National Key R&D Program of China, Grant/Award Number: 2019YFC1906702; National Natural Science Foundation of China, Grant/Award Numbers: 91834301, 22078088; Shanghai Rising-Star Program, Grant/Award Number: 21QA1401900

Abstract

Development of porous electrode materials for high-performance supercapacitors depends on the efficiency of pore utilization for charge storage. It remains an experimental and theoretical challenge to quantitatively relate the porous structure to charging dynamics. Here, based on a laminate-electrode model of graphene-based supercapacitors, we perform the equivalent circuit model to characterize the structure-charging dynamics relationship of porous electrodes by coupling key structural features in a mathematical expression for the Resistor-Capacitor (RC) time. This theoretical description is validated by direct numerical calculations of the Poisson–Nernst–Planck (PNP) equations. We discover that the charging dynamics of graphene-based supercapacitors is dominated by the ion diffusion from the electrolyte region into the layered structure. The predicted charging time compares well with the experimental investigations reported in the literature on graphene-based supercapacitors. Our work bridges nanoscopic transport behaviors with macroscopic devices, providing theoretical insights of the structure-dependent ion transport in two-dimensional materials-based films for compact energy storage.

KEYWORDS

charging dynamics, equivalent circuit model, laminate-electrode model, Poisson–Nernst–Planck equations, supercapacitor

1 | INTRODUCTION

Supercapacitors store energy by forming electric double layers (EDLs) through reversible ion adsorption on the surface of porous electrodes.[1] With high power density, long cycling life, and safe operation, supercapacitors have shown great promise for portable electronics and electric vehicles,[2,3] but their practical applications are limited by their relatively poor energy density.[4] The energy density of existing commercialized supercapacitors, which are mainly based on porous activated carbon (AC),[5] is far lower than that of batteries. For electrochemical double layer capacitors (EDLC), both broadening the operation potential window (U) and increasing the specific capacitance (C) can improve the energy density.[6] The U depends substantially on the choice of electrolytes, such as aqueous electrolytes (0–1 V), organic electrolytes (2–4 V) and ionic liquids (~4 V).[7,8] Increasing the efficiency of pore utilization to store charge in porous electrodes is essential to enhance C.[9] A variety of carbon nanomaterials can serve as nanoscale building blocks to create complex functional architectures for high-performance supercapacitors.[10] For instance, graphene-based electrodes, which align two-dimensional (2D) graphene-based nanosheets into highly compact layered film structures, enable the interlayer spacing to be more effectively utilized for storing charges.[11–13] With the highly compact form of the electrode structure, the layered graphene-based supercapacitor can deliver an outstanding energy density, but the transport and accessibility of ions will be less efficient, which may lead to decreased power density.[14] The power density can be promoted by increasing the U and reducing the global resistance (R) of the supercapacitor, and the latter can be achieved by regulating the layered structure of graphene-based electrodes. Therefore, a good assembly of the 2D nanosheets is significant

for building better electrodes with high energy and power output,[15,16] which requires a deep understanding of the relationship among layered structure, capacitances, and charging dynamics. While most reported theoretical studies focused on calculating the capacitances, it is also important and relevant to study the charging dynamics.

To establish a comprehensive structure-charging dynamics relationship of graphene-based electrodes, we can describe their complex structure by several simplified and statistically representative elements in a laminate-electrode model. Generally, the micro-structure of the layered graphene-based membranes can be represented by an array of cascading nanoslits through parallel stacking multiple graphene nanosheets with three key geometrical variables (namely, the interlayer spacing h, the in-plane pore sizes δ and the distance between the adjacent pores l).[17,18] The relatively regular structure of a layered graphene-based electrode is different from the highly disordered structure in a carbide-derived carbon (CDC) electrode that is widely used in carbon-based supercapacitors, both of which are well compared in a theoretical study of Méndez-Morales et al.[19] It is found that hierarchical nanoporous structures of the CDC electrode allow co-ions to move away from surfaces, leading to an increased capacitance. In the laminate-electrode model, the pore size δ specifies the holes distributed in the graphene sheets as well as the gap between the adjacent graphene sheets. By contrast, the layer spacing h is similar to the defined pore size in the typical disordered nanoporous carbon,[20,21] which is a dominant factor that can be adjusted to match the electrolyte ions to reach a better capacitance.[22] Recently, a free-standing graphene laminate film with tuneable interlayer spacing has been developed for efficient pore utilization, which is composed of graphene oxide with a controlled amount of exfoliated graphene.[14] The interlayer spacing is finely tuned by changing the ratio of the two precursors. Pillared graphene-based materials can also optimize the interlayer separation and limit restacking of graphene sheets by controlling the pillars inside the graphene galleries, and thus showing efficient charge storage.[23–25] The pore-to-pore distance l is a key geometrical parameter that determines the tortuous transport pathways of ions in the layered electrodes. As demonstrated in previous research,[17] the increase in l and the decrease in δ enhance the barrier properties of the layered graphene-based membranes. To facilitate the transport and accessibility of ions in the highly compact form, a holey graphene framework with smaller l was constructed through H_2O_2 etching, which delivers high gravimetric and volumetric energy densities.[26] Although several assembly strategies for the graphene-based electrodes have been implemented to achieve outstanding compact energy storage,[12,26,27] it is still unclear whether the established porous structure is optimal for the charging dynamics and charge storage.

Currently, in situ experimental techniques (NMR spectroscopy, electrochemical quartz crystal microbalance (EQCM), infrared (IR) spectroscopy, and scattering approaches),[28,29] and simulation techniques including molecular dynamics (MD) simulation[30–34] and classical density functional theory (CDFT),[22,35,36] can elucidate the EDL buildup at the electrode/electrolyte interface and the charging mechanisms in individual nanopores as well as disorder carbon materials. It was shown that the mechanisms of charge storage and ion transport are sensitive to both pore size[37,38] and local porous structure.[39–41] Both current experimental techniques[42,43] and molecular simulations[44,45] can account for the structural complexity of porous carbon electrodes to some extent, but they are also limited: the former needs an accurate description of the structure on the atomistic scale and the latter requires a high computational cost for a realistic system containing a large number of atoms.[29] It is demonstrated that highly-ordered carbon materials such as graphene-based electrodes can serve as a model system to probe structure–property relationships.

In this work, we aim to describe the charging behavior in the laminate-electrode model of the graphene-based supercapacitors through an equivalent-circuit model and direct numerical calculations, focusing on discussing the roles of structural variations of the laminate-electrode model in the charging dynamics systematically. The equivalent-circuit model has been widely used in modeling the physical components of an electrochemical device with circuit element representations. Therefore, it is used to give a representative description for the laminate-electrode model, as well as quantify the charging rate by defining a relaxation timescale that contains specific geometrical parameters. The direct numerical calculations of the Poisson–Nernst–Planck (PNP) equations are implemented to directly describe the structure-dependent charging process in the laminate-electrode model, providing data support to verify and optimize the expression of the relaxation timescale, simultaneously revealing the charging characteristics at the microscale and high potentials which cannot be described accurately by the equivalent circuit model. Finally, this quantitative characterization of the charging time for graphene-based supercapacitors is validated through a comparison between theoretical prediction and experimental evaluation.

2 | RESULTS AND DISCUSSION

2.1 | Laminate-electrode model

A simple but representative micro-structure model is important for the theoretical study and for understanding the relationship of the bulk performance of the nano-porous structure. Here, as shown in Figure 1A, we construct a model of the graphene-based supercapacitor containing a 1:1 electrolyte, two laminate film-based electrodes of thickness H separated by a surface-to-surface distance of $2L$. In the laminate-electrode model (Figure 1B), both the cathode and the anode are composed of n parallel graphene sheets, in which nanopores of pore size δ are distributed evenly at intervals of $2l$. Considering that we solve a 2D system for the laminate-electrode model, the so-called nanopores can directly represent the slit-like gaps between the ends of adjacent graphene sheets, and approximately describe the cylindrical holes evenly distributed in the graphene sheets. The interlayer spacing of adjacent sheets is h, and the thickness of the electrode equals $H = (n-1)h$. Once an electric field is applied, ions from the electrolyte can enter and leave the layered structure of the electrode,

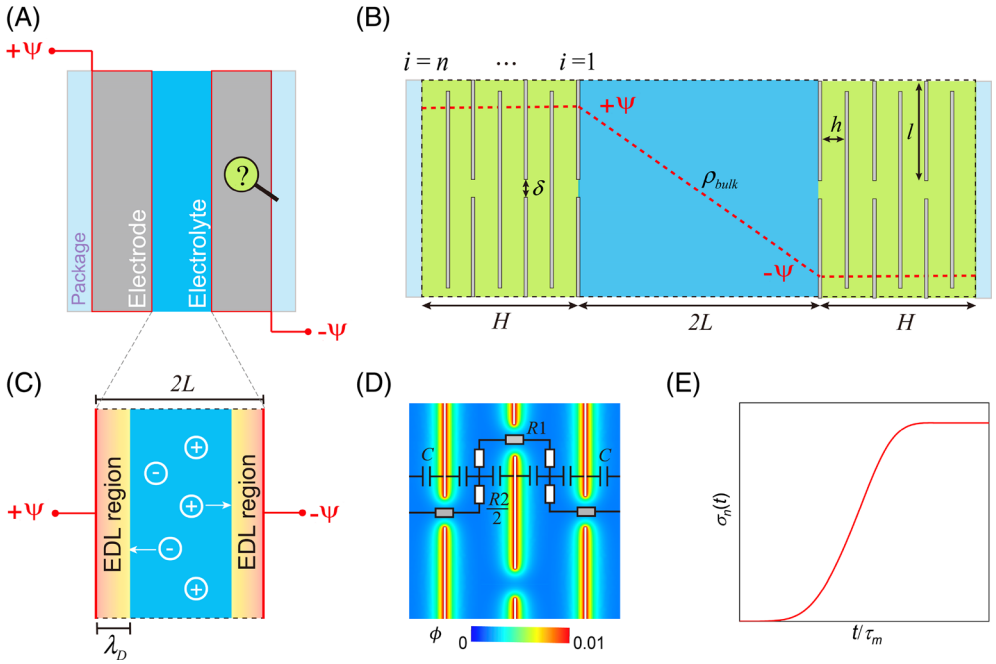

FIGURE 1 (A) Schematic diagram illustrating the composition of a film-based supercapacitor. It is important to present the complex inner structure of the electrodes. (B) Sketch of a model for the graphene-based supercapacitor with two laminate film electrodes. The cathode and anode each contain n graphene sheets with interlayer spacing h, pore size δ, and distance l between the adjacent pores. The initial anionic and cationic concentrations in the 1:1 electrolyte are ρ_{bulk} throughout the cell. After time $t = 0$, nonzero potentials $+\Psi$ and $-\Psi$ are applied to all sheets on the left and right-hand side of the system, respectively. (C) Sketch of the plate electrode system, which can be used to describe the laminate-electrode model in the trivial case $n = 1$. Ion transport from the bulk electrolyte to the electrode surface takes place, leading to the formation of electrical double layers (EDLs), where $2L$ is the electrode spacing and λ_D is Debye screening length (EDL thickness). (D) Equivalent circuit with resistors and capacitors for the local layered structure of the graphene-based supercapacitor. (E) The surface charge $\sigma_n(t)$ at the $i = n$ sheet of the laminate-electrode model forms exponentially, where the time evolution t can be scaled by the relaxation timescale τ_m to obtain a structure-independent charging profile.

subsequently adsorb/desorb at the inside electrode surfaces to form the EDLs that screen the applied potentials. The equilibrium thickness of the EDL is characterized by the Debye length $\lambda_D = \kappa^{-1} = \sqrt{\varepsilon k_B T/(2e^2\rho_{bulk})}$, with ρ_{bulk} the bulk ion number density, ε the electrolyte permittivity, e the elementary charge, and k_BT the thermal energy. The structure model with the geometrical parameters of h, l, and δ is reliable for describing the complex structure of layered graphene-based membranes, which is validated quantitatively by experimental research.[17,46] In these experiments, the layered graphene-based films are assembled by aligning the multiple graphene-based nanosheets into a self-similar, layered configuration that allows the average interlayer spacing to be continuously adjusted in a range from about 10 nm to sub-nanometer, which can be represented by the laminate-electrode model structurally.

The laminate-electrode model is used to study the geometrical influence of the graphene-based supercapacitor in the charging dynamics, but does neither consider the atomic and electronic structure of graphene,[47] nor the ion–ion interaction across carbon sheets,[48,49] which can be studied using the molecular simulations and electronic density functional theory. For example, an atomic model for the layered graphene-based supercapacitor with the electrolyte of BMIM-PF_6 was established by Mendez-Morales et al.,[50] showing that ion–ion correlations exist under strong confinement, both across and between electrified graphene layers. These correlations were attributed to the strong localization of image charges on the carbon atoms. It is also worth noting that the EDL capacitance is suppressed by the low density of states of the graphene electrode near the point of zero charge (PZC), but enhanced by the electrostatic correlation effects between electrons in the graphene sheet and the electrolyte ions between the sheets.[51] The quantum capacitance also plays an important role in the total capacitance, but the effects may be different for specific systems.[52,53] In short, these effects related to the intrinsic properties of graphene are ignored in the laminate-electrode model, and we focus on solving the diffusion and migration processes in the layered geometry as inspired by the graphene-based supercapacitor.

2.2 | Quantify charging process using equivalent circuit model

First, to give a vivid description of the effect of these geometrical variables on the charging process of the laminate-electrode model for graphene-based electrodes, the equivalent circuit model (ECM) is introduced. The ECM for a minimal one-dimensional (1D) stack-electrode model has been reported, which can approximately describe the charging dynamics of porous carbon electrodes.[54–56]

However, our electrode model describes specific micro-structural characteristics of the laminated film beyond the pore size. Thus, the ECM of the simple planar (1D) model is extended to include more structural elements of our 2D model. According to the ECM, the established supercapacitor can be modeled as an Resistor-Capacitor (RC) transmission line,[57] in which the case of a simple planar electrode ($n = 1$) is firstly discussed as shown in Figure 1C. For simplicity, the interfacial charge storage at the EDLs on each sheet is described by the Helmholtz model with a capacitor of capacitance $C = A\varepsilon\kappa$, where A is the surface area facing the electrolyte, ε the electrolyte permittivity and κ^{-1} the Debye length, but it is worth noting that the capacitance depends on the electrical potential and ion density. The ion transport resistance through the electrolyte is modeled with a resistor of resistance $2R = 2L/(A\varepsilon\kappa^2 D)$, where D is the ion diffusivity that we take equal for the cations and anions for simplicity. As derived in Method section, the relaxation time for the planar electrode can be expressed as:[58,59]

$$\tau_{RC} = RC = \frac{\lambda_D L}{D}. \quad (1)$$

Inserting calculation parameters $\kappa^{-1} \approx 1\,\text{nm}$, $L \approx 200\,\text{nm}$ and $D \approx 1\,\text{nm}^2\,\text{ns}^{-1}$, yields $\tau_{RC} = 200\,\text{ns}$. The detailed discussion for the ECM and relaxation times is given in Supplementary Information. For the case of electrodes composed of $n > 1$ layers, additional capacitors and resistors are introduced into the circuit. Similarly, the outermost capacitors have a capacitance C, while all inner capacitors have 2C, as they mimic electrodes with electrolyte on either side. Therefore, the overall capacitance of the laminate-electrode model of n layers is expressed as $C_m = (2n-1)C$, where the subscript m refers to membrane character of an electrode with n layers considered. As shown in Figure 1D, the ion transport resistance through the electrolyte between adjacent capacitors are divided into two resistors R_1 and R_2, which is different from the previous planar 1D model that did not include the tortuous transport pathways in the porous electrode.[54] The resistor R_1 is expressed as $R_1 = h/(A\varepsilon\kappa^2 D)$ with A the surface area facing the electrolyte, which represents the ion transport resistance perpendicular to the surface with the distance of interlayer spacing h. The resistor R_2 is expressed as $R_2 = l/(A'\varepsilon\kappa^2 D)$ with A' the sectional area of the slit pore, which represents the ion transport resistance along the sheets with the distance between the adjacent pores of l. Then, with $A'/A = h/l$, we get the overall resistance for the general n case of each film electrode: $R_m = R + (n-1)(R_1 + R_2)$, where R is the resistance of a half of the electrolyte separating the two membrane electrodes as calculated in the case of $n = 1$. The overall relaxation timescale for the laminate-electrode model is calculated by:

$$\tau_m = R_m C_m = (2n-1)\left[1 + \left(1 + \frac{l^2}{h^2}\right)\frac{H}{L}\right]\tau_{RC}, \quad (2)$$

which is carefully discussed in Supplementary Information. The relaxation time τ_m quantifies the charging rate of the whole process, as shown in Figure 1E, which is largely determined by the microscopic structure of porous electrodes except the properties of electrolyte and the architecture of the macroscopic device. According to Equation (2), for the same thickness of the electrolyte layer (L), it is found that $\tau_m \propto n^2$ at fixed h and l, as well as $\tau_m \propto l^2$ at fixed n and h, which means that the system has a larger relaxation time with increasing n and l. With n and l fixed, $\tau_m \propto \left(h + l^2/h\right)$, which indicates that the charging dynamics slows down with decreasing h for typical $h < l$. Moreover, to involve the effect of bulk concentration, the dimensionless length scales including κH, κL, κl, and κh, with respect to the Debye length κ^{-1} are used during the following discussion.

2.3 | Structure-dependent charging dynamics

With the above laminate-electrode geometry for graphene-based supercapacitors, the PNP equations are used to solve the dynamics of the mass transport of solution species under the effects of diffusion and migration. The PNP equations implicitly assume all dissolved species to be point particles, an approximation that breaks down at high concentrations, for instance, at concentrated bulk solutions or close to charged surfaces at high potentials where steric effects become important. Therefore, we perform the PNP calculations at small potentials and low concentrations to make it reliable for describing our system. Nevertheless, the description for the charging process at mild conditions can also help us understand the practical supercapacitors at high concentrations and large potentials, as demonstrated in a recent study on charging dynamics,[60] which uses a classical dynamic density functional theory that accounts for electrostatic correlations and for the molecular excluded volume of finite-sized ions and solvent molecules. Importantly, the PNP-based model allows us to quickly solve the ion transport in systems with length scales of a micron and time scale between picoseconds and seconds, which is rather efficient for investigating the influence of all the structural parameters on the charging process.

In Figure 2A, we present the numerical results for the time-dependent potential distributions in the model of the graphene-based supercapacitor. The initial anionic and cationic concentrations in the 1:1 electrolyte are $\rho_{bulk} = 0.1\,\text{M}$ throughout the cell, which correspond to the equilibrium concentration at zero voltage (at times $t < 0$) for the calculations of PNP equations. At time $t = 0$, the dimensionless potential difference 2ϕ, measured in units of the thermal voltage $k_B T/e$ ($\approx$25 mV), is applied to the anode and cathode of the supercapacitor. As time goes on, cations and anions are driven by the electric field to enter and leave the layered structures of the laminated electrodes from the bulk electrolyte gradually. The counter-ions adsorb on the electrode surface and the co-ions desorb from them such that the EDLs form, which screens the surface potentials, as shown in the zoom-in diagrams of both anode and cathode at the bottom of Figure 2A. The surface charge density σ_i of the individual sheet i, which is calculated by the Gauss' law $\sigma_i(t) = \varepsilon k_B T(-n \cdot \nabla\phi_i(t))/e$, is plotted in Figure 2B as a function of the dimensionless time t/τ_{RC}. Sheets closer to the reservoir charge up faster initially, but all sheets almost reach 99% of the equilibrium charge at about the same time around $t/\tau_{RC} = 8000$. In Figure 2C, the charging relaxation $1 - \sigma_i(t)/\sigma_{eq}$ of different sheets, where $\sigma_{eq} \equiv \sigma_i(t/\tau_{RC} \to \infty)$ is the late-time

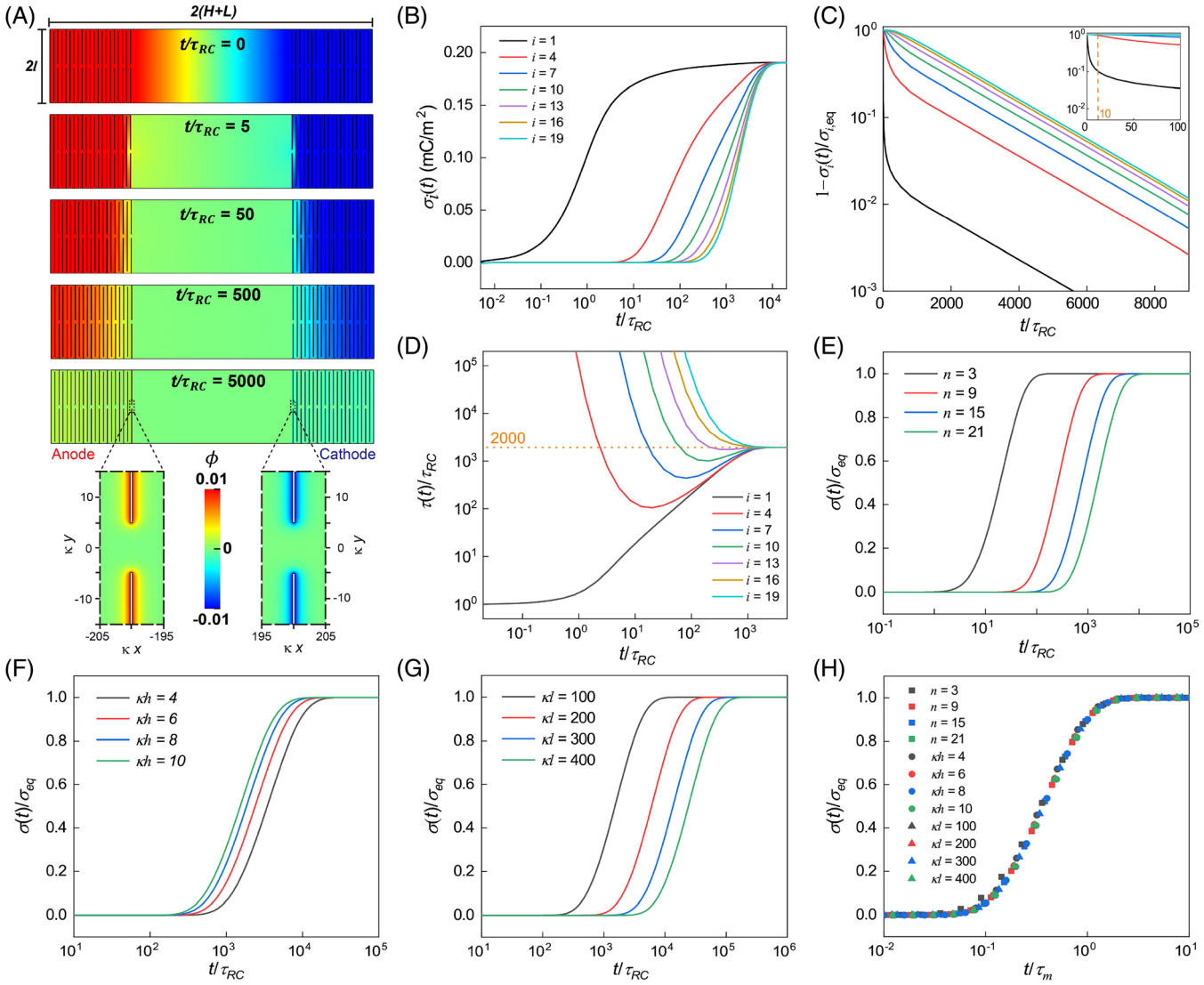

FIGURE 2 (A) The potential distributions in the model of the graphene-based supercapacitor upon applying an extremely low potential $\phi = 0.01$ in units of the thermal potential, for system parameters $n = 21$, $\kappa\delta = \kappa h = 10$, $\kappa l = 100$, and $\kappa L = 200$ at times $t/\tau_{RC} = 0$, 5, 50, 500, and 5000. Time dependence of (B) the surface charge density $\sigma_i(t)$, (C) the charging relaxation $1 - \sigma_i(t)/\sigma_{i,eq}$, and (D) the time-dependent (dimensionless) decay rate $\tau(t)/\tau_{RC}$ at the graphene sheets labeled by $i = [1, 4, 7, 10, 13, 16, 19]$ with $i = 1$ the innermost sheet. The dependence of the surface charge density $\sigma(t)/\sigma_{eq}$ of the outermost electrode ($i = n$) from the numerical calculation at (dimensionless) potential $\phi = 0.1$ for (E) $n = [3, 9, 15, 21]$, (F) $\kappa h = [4, 6, 8, 10]$ and (G) $\kappa l = [100, 200, 300, 400]$ on the charging time scaled by τ_{RC}. The default values of these parameters are $n = 21$, $\kappa\delta = \kappa h = 10$ and $\kappa l = 100$ unless we adjust one of them. (H) Collapsed time-dependent profiles if time is measured in units of τ_m as derived by the ECM in Equation (2).

surface charge density, presents different delay behaviors. The charging relaxation of the $i = 1$ sheet that directly faces the bulk electrolyte has two processes. As shown in the inset figures of Figure 2C, when $t/\tau_{RC} < 10$, the curve $1 - \sigma_i(t)/\sigma_{eq}$ of the $i = 1$ sheet drops down to 10% sharply and decreases slowly at late times. By contrast, at early times the relaxation process of sheets $i > 1$ are always much slower than the $i = 1$ case, and the slower the deeper inside the electrode. At late times, $1 - \sigma_i(t)/\sigma_{eq}$ of all these sheets decreases exponentially with the same time constant. To characterize the different time response during the relaxation process, according to a purely exponential charge buildup $\sigma(t) = \sigma_{eq}[1 - \exp(-t/\tau)]$, a time-dependent function $\tau(t)$ is defined:[54]

$$\tau(t) = -\left[\frac{d\ln(1-\sigma(t)/\sigma_{eq})}{dt}\right]^{-1}, \quad (3)$$

which yields the instantaneous relaxation time scale $\tau(t)$ for different charge relaxation stages. Accordingly, as shown in Figure 2D, for the $i = 1$ sheet, we can find that $\tau = \tau_{RC}$ at early times ($t/\tau_{RC} < 1$), which is a standard RC time, while τ rises gradually to $2000\tau_{RC}$ at late times ($t/\tau_{RC} > 1000$). The slower relaxation timescale $\tau = 2000\tau_{RC}$ at the second plateaus is equal to $L^2/(\pi^2 D)$, which is a slow diffusion timescale.[58,61] However, for the sheets far away from the bulk electrolyte ($i > 1$), only the second plateaus can be observed, since the charging process is dominated by the ionic diffusion due to

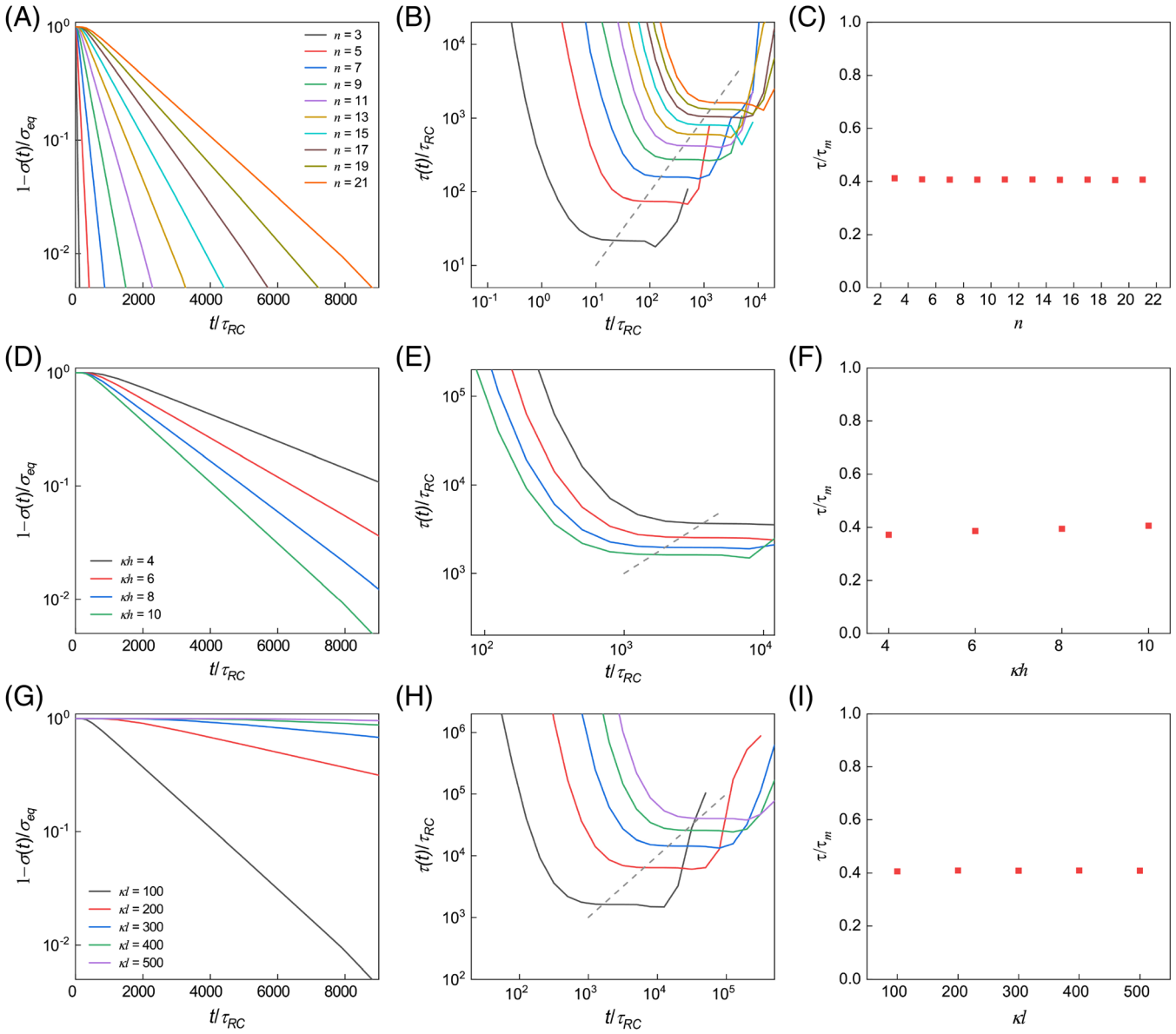

FIGURE 3 The dependence of the charging relaxation $1-\sigma(t)/\sigma_{eq}$ and time-dependent function $\tau(t)/\tau_{RC}$ for outermost electrode ($i=n$) from the numerical calculation at $\phi=0.1$ for (A,B) $n=3$–21, (D,E) $\kappa h=[4, 6, 8, 10]$ and (G,H) $\kappa l=[100, 200, 300, 400, 500]$ on the charging time that scaled by τ_{RC}. The default values of these parameters are $n=21$, $\kappa h=10$, and $\kappa l=100$ unless we adjust one of them. The ratio of the timescale τ calculated by numerical calculations to the timescale τ_m derived by the ECM for the geometrical parameter (C) n, (F) κh, and (I) κl.

the tortuous transport pathways inside the graphene-based electrode.

To explore the structure-charging dynamics relationship of the laminated electrodes, we perform numerical calculations in the laminate-electrode model with different geometrical parameters. The surface charge density $\sigma(t)/\sigma_{eq}$ of the outermost sheet ($i=n$) as a function of the charging time t/τ_{RC} is plotted in Figure 2E–G. With the increase of the n at fixed layer spacing h and pore–pore separation l (Figure 2E), the duration time of the charging process is longer due to the larger thickness of the electrode. We can see from Figure 2F that the charging dynamics slows down with decreasing h although the thickness of the electrode is reduced at fixed n and l, which may be attributed to the increasing nano-confinement. The increase of l alone results in a longer pathway for ions to transport from one interlayer to another, which also slows down the charging dynamics (Figure 2G). Therefore, we found the influence of these geometrical parameters on the charging dynamics from numerical calculations to be consistent with that from our qualitative analysis from the ECM according to the Equation (2). To better understand these phenomena, we scale time by the timescale τ_m as derived by the ECM above, and plot these time-dependent profiles of the surface charge density $\sigma(t)/\sigma_{eq}$ with different geometrical parameters together in Figure 2H. Interestingly, we can see that all these curves collapse into one master curve, which indicates that the timescale τ_m can provide a quantitative

expression to describe the charging dynamics in the laminate-electrode model well. This phenomenon is also indicated in the collapsed time-dependent profiles of the charging relaxation $1-\sigma(t)/\sigma_{eq}$ as shown in Figure S3.

Furthermore, in Figure 3, we also show the charging relaxation $1-\sigma_i(t)/\sigma_{eq}$ and time-dependent function $\tau(t)/\tau_{RC}$ as a function of the charging time t/τ_{RC} with changing the geometrical parameters n, κh, and κl. As shown in Figure 3A,D,G, only one relaxation timescale for each geometrical configuration can be observed, which is dominated by the ionic diffusion rather than the build-up of EDLs as discussed above. We also can see that increasing n and κl, as well as decreasing the κh are not favorable for the charging dynamics. To quantify the timescale of the relaxation process, we calculate the negative reciprocal values of the first derivative of the charging relaxation profiles using Equation (3), as plotted in Figure 3B,E,H, where the value of the plateaus is considered as the timescale τ. Furthermore, for different geometrical parameters, a comparison between the timescale τ from the numerical results and the timescale τ_m from the ECM is implemented as shown in Figure 3C,F,I, and we find a constant relation $\tau/\tau_m \approx 0.4 \approx 4/\pi^2$.[61] Hence, we define a modified timescale,

$$\tau_{2D} = \frac{4}{\pi^2}\tau_m = \frac{4}{\pi^2}(2n-1)\left[1+\left(1+\frac{l^2}{h^2}\right)\frac{H}{L}\right]\tau_{RC}, \tag{4}$$

to describe the charging dynamics in the laminate-electrode model.

2.4 | Charging dynamics at nano-confinement

The quantitative comparison between the numerical calculations and the ECM analysis as discussed above, is largely based on an unconstrained system (large $\kappa\delta$ and κh) in which the EDLs are fully developed without any overlap. In practical supercapacitors, due to crowding and intermolecular forces under severe nano-confinement, the transport behavior of ions can be influenced by the interfacial EDL induced by a surface potential, with complex implications and unconventional ion dynamics.[46,62] Therefore, we cannot ignore the nano-confinement (small $\kappa\delta$ and κh) into the laminated electrode for the study of the charging dynamics. It is worth noting that the PNP equations are not applicable for the sub-nanometer scale, which ignores the spatial confinement effects arisen from strong ion-wall interactions and steric restrictions, but which can describe the ion transport in the layered graphene-based structure with sub-10-nm tuneable interlayer spacing. As indicated in the research of Cheng et al.,[17] diffusive transport has a high level of consistency between experiment and numerical simulation of ion diffusion through the model structure as the interlayer spacing varies across the entire range from 10 to ~1 nm. Moreover, the continuum framework has also been proven to be robust when applied to the description of nanoscale transport phenomena at a level of confinement larger than ~1 nm.[63,64] Accordingly, we further provide a description of the charging dynamics in a relatively constrained system of $\kappa\delta$ and κh varying from 1 to 20, which mainly present the effect of the EDL structure in the confined space.

The pores and defects on the graphene sheets determine the transport of ions from one interlayer space to another, and thus play an important role in the charging dynamics.[65] To investigate the effect of pore size on the charging dynamics, which is difficult to consider in the ECM directly, we perform numerical calculations with the pore size $\kappa\delta$ varying from 1 to 20. Herein, ion transport can be driven by the applied potential and by concentration differences between bulk electrolyte and interlayer spacing. The former leads to charge separation in the layered structure, and many counter-ions from the bulk electrolyte will go through the one-by-one interlayer spacing until adsorbed on the inner electrode surface. As shown in Figure 4A, with the decrease of the pore size, the EDLs at the edges of the sheets tend to overlap, which results in a high accumulation of counter-ions near the pore area. The reverse concentration gradient against the transport direction increases the resistance of ion transport through the nanopores.Therefore, we can explicitly see from Figure 4C that the charging dynamics slows down for smaller pore size. Meanwhile, we find that curves of the surface charge density $\sigma(t)/\sigma_{eq}$ on the charging time scaled by τ_{2D} cannot coincide with each other (Figure 4D), since the structural variable $\kappa\delta$ is not involved in the formulation of τ_{2D} from ECM. The quantitative contribution of the pore size $\kappa\delta$ on the charging process is considered by numerically calculating the timescale τ_δ using Equation (3) to compare with the derived timescale τ_{2D}. As shown in Figure 4E, to quantify the difference of τ_δ and τ_{2D}, we present the relative timescale τ_δ/τ_{2D} as a function of the pore size $\kappa\delta$. The smaller pore size, the larger the deviation of τ_{2D} compared to τ_δ. The value of τ_δ/τ_{2D} approaches 1 when $\kappa\delta > 10$, which means that the confinement of interlayer spacing can be ignored. In addition, we find these plots to resemble the purely phenomenological function $1+\exp(-\kappa\delta/2)$. Consequently, the timescale τ_{2D} can be further optimized through multipying it by the variable

$$\alpha = \frac{\tau_\delta}{\tau_{2D}} = 1+\exp\left(-\frac{\kappa\delta}{2}\right), \tag{5}$$

which includes the effect of (small) δ.

The interlayer spacing κh is a key parameter in determining the EDL capacitance. To get insight into the influence of κh on the charge distribution inside the laminated electrode, we present local distributions of space charge density in an area of 20×20 with $\kappa h = [1, 2, 5, 10]$ in Figure 4B. When $\kappa h = 1$, the EDLs overlap completely, which means that there is not enough space to store the possible charges given the applied potential. Hence, to increase the capacitance, we can broaden the interlayer spacing to fill the EDLs fully. However, with increasing κh to more than 5, two-face-to face (almost) fully developed EDLs are separated, and meanwhile a neutral region between two adjacent sheets appears. This case is not favorable for efficient pore utilization because the neutral region is flooded by the electrolyte, which has however no contribution to the capacitance while increasing the weight and the resistance of the entire device. Furthermore, as shown in the Figure 4F, we plot the surface charge density as a function of the time scaled by τ_{RC} with the κh varying from 1 to 10. The surface charge density at steady states increases

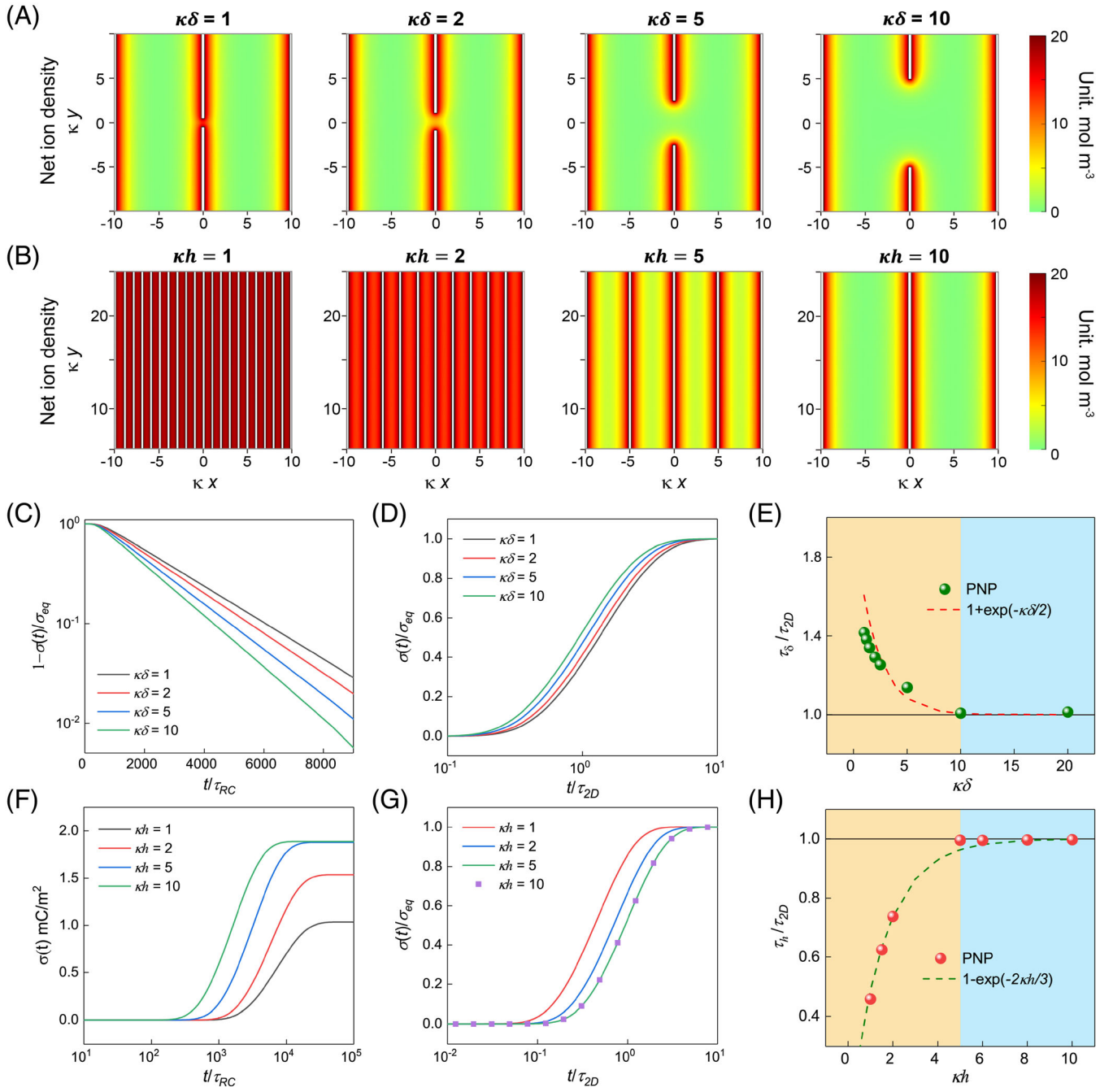

FIGURE 4 The local distributions of net ion density in the area (20 × 20) near a nanopore with (A) different pore sizes $\kappa\delta = [1, 2, 5, 10]$ for $\kappa h = 10$ and (B) different interlayer spacing $\kappa h = [1, 2, 5, 10]$ for $\kappa\delta = 10$, both in steady states for applied (dimensionless) potentials $\phi = 0.1$, $n = 21$, $\kappa l = 100$, and $\kappa L = 200$. (C) The charging relaxation $1 - \sigma(t)/\sigma_{eq}$ for $\kappa\delta = [1, 2, 5, 10]$ on the charging time that scaled by τ_{RC} in steady states. (D) The surface charge density $\sigma(t)/\sigma_{eq}$ for the outermost electrode ($i = n$) as a function of time scaled by the timescale τ_{2D} with different pore sizes. (E) The ratio of the timescale τ_δ at $\kappa\delta = [1, 1.2, 1.5, 2, 5, 10, 20]$ calculated by numerical calculations to the corresponding timescale τ_{2D}. (F) The dependence of surface charge density $\sigma(t)$ for $\kappa h = [1, 2, 5, 10]$ on the charging time that scaled by τ_{RC} in steady states. (G) The surface charge density $\sigma(t)/\sigma_{eq}$ for the outermost electrode ($i = n$) as a function of time scaled by the timescale τ_{2D} with different interlayer spacing. (H) The ratio of the timescale τ_h at $\kappa h = [1, 2, 5, 6, 8, 10]$ calculated by numerical calculations to the timescale τ_{2D}.

with a larger interlayer spacing, and then keep constant when $\kappa h > 5$, in which the overlap of EDLs disappears. The interlayer spacing κh also plays an important role on the charging dynamics. We can find that increasing the interlayer spacing is favorable for the charging process. To verify the accuracy of the timescale τ_{2D} on describing the charging process in a narrow interlayer space, we plot the surface charge density $\sigma(t)/\sigma_{eq}$ with the time scaled by τ_{2D} for $\kappa h = [1, 2, 5, 10]$ in Figure 4G. We can see that the lines for $\kappa h < 5$ do not coincide with each other, which indicates that the timescale τ_{2D} cannot describe the relaxation time of the cases when the EDLs overlap

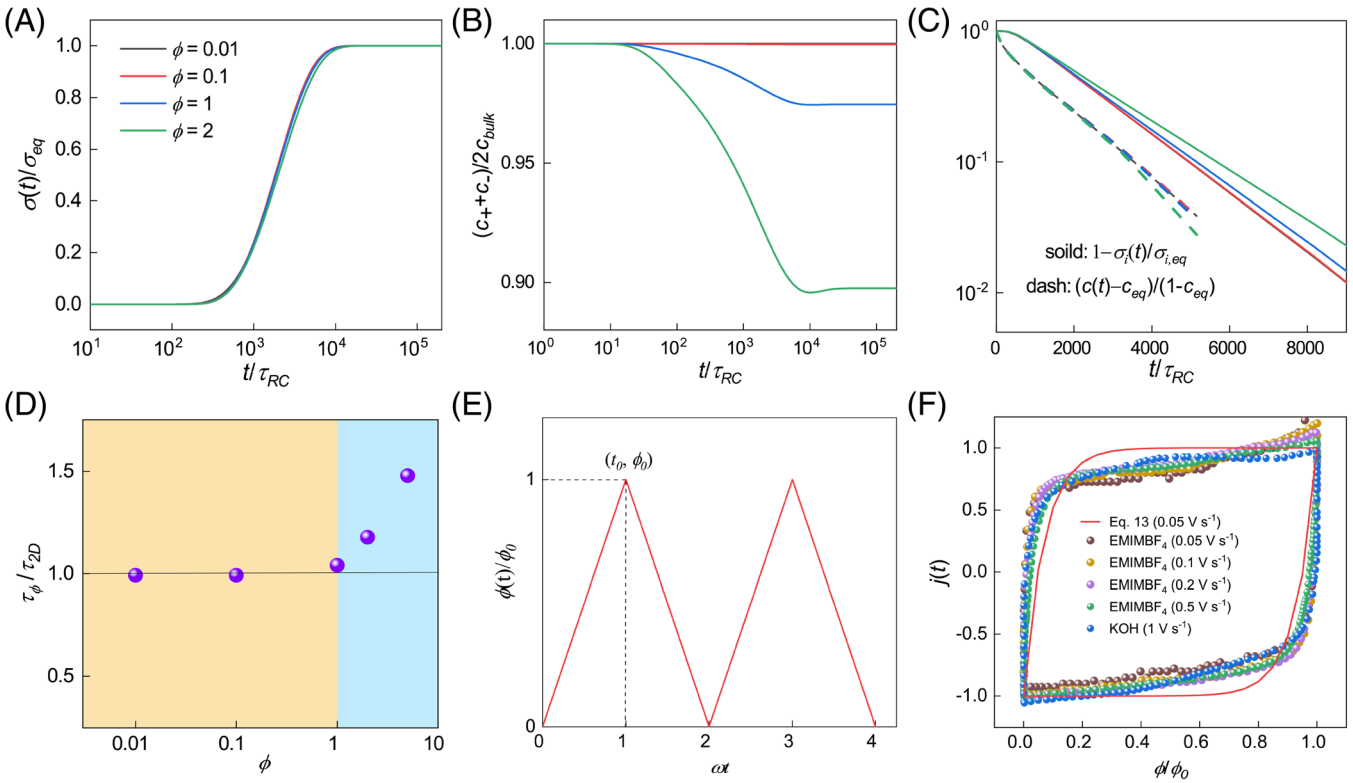

FIGURE 5 (A) The surface charge density $\sigma(t)/\sigma_{eq}$, (B) the cell-center salt concentration $c(t) = (c_+ + c_-)/2c_{bulk}$, (C) the charge relaxation $1 - \sigma_i(t)/\sigma_{eq}$ (solid lines) and the concentration delay $(c(t) - c_{eq})/(1 - c_{eq})$ (dashed lines) of the laminate-electrode model for $i = n = 21$, $\kappa L = 200$, $\kappa l = 100$, and $\kappa\delta = \kappa h = 10$ at dimensionless potentials $\phi = [0.01, 0.1, 1, 2]$. (D) The ratios of the timescale τ_ϕ at potentials $\phi = [0.01, 0.1, 1, 2, 4]$ calculated by numerical calculations to the corresponding timescale τ_{2D}. (E) The nondimensionless saw-tooth potential $\phi(t)/\phi_0$ that is used in CV experiments and in the ECM, where $\omega = 1/t_0$ is the scan frequency. (F) Comparison of the circuit model (red line) for aqueous electrolyte at the scan rate of 0.05 V s^{-1} corresponding to $\omega = 0.05$ s^{-1} when $\phi_0 = 1$ V, and the experimental data (color dots) for the organic electrolyte ($EMIMBF_4$) at the scan rate of 0.05, 0.1, 0.2, 0.5 V s^{-1} ($\phi_0 = 3.5$ V) and the aqueous electrolyte (6 M KOH) at the scan rate of 1 V s^{-1} ($\phi_0 = 1$ V). The experiment data are from the previous research[26] of Xu et al. on the holey graphene framework.

significantly. Moreover, it reveals that τ_{2D} overestimates the charging time, the more so for smaller interlayer spacing. Like the discussion about $\kappa\delta$ above, we further quantify the difference of the timescale τ_h obatined from numerical calculations and the τ_{2D}, as the relative timescale τ_h/τ_{2D} shown in Figure 4H, and thus for small interlayer spacings, the timescale τ_{2D} can be optimized by including the coefficient:

$$\beta = \frac{\tau_h}{\tau_{2D}} = 1 - \exp\left(-\frac{2\kappa h}{3}\right). \tag{6}$$

All in all, for the laminate-electrode model, an optimal interlayer spacing can be found not only to promote the charge separation but also to allow the faster ion diffusion, such as $\kappa h = 5$ here, which is favorable for both the EDL capacitance and the charging dynamics.

2.5 | Theoretical prediction versus experimental evaluation

Because supercapacitors are typically subjected to large potentials in practical applications, we also study the charging dynamics of the laminate-electrode model at high (dimensionless) potentials $\phi > 1$. In Figure 5A–C, we present the numerical results for $n = 21$, $\kappa L = 200$, $\kappa l = 100$ and $\kappa\delta = \kappa h = 10$ at potentials $\phi = [0.01, 0.1, 1, 2]$. The normalized surface charge density $\sigma_i(t)/\sigma_{eq}$ develops slightly slower at high potentials as shown in Figure 5A. Moreover, Figure 5B shows the cell-center salt concentration $c(t) = (c_+ + c_-)/2c_{bulk}$ at these potentials. At $\phi < 0.1$, we find $c(t) = 1$. However, at $\phi = 1$ and 2, it is found that $c(t)$ decreases by 3% to 10% at the later time ($t/\tau_{RC} > 10^4$) due to the ionic transport from the bulk electrolyte to the electrode surface in the closed system. Furthermore, we show the charge relaxation $1 - \sigma_i(t)/\sigma_{eq}$ (solid lines) and the concentration delay $(c(t) - c_{eq})/(1 - c_{eq})$ (dashed lines) in Figure 5C, where $c_{eq} \equiv c(t/\tau_{RC} \to \infty)$. We find the slopes of $1 - \sigma_i(t)/\sigma_{eq}$ ($i = 21$) and $(c(t) - c_{eq})/(1 - c_{eq})$ are the same for all ϕ considered, which also demonstrates that the charging process is dominated by the ionic diffusion. The charging relaxation is slower than the cell-center concentration delay due to the tortuous transport pathways through the layered membrane. Furthermore, we can find from Figure 5D that the difference of τ and τ_{2D} is larger for higher potential. It is noted that the considered potential here is higher only compared to the previous discussion but is still quite low than the potentials in practical supercapacitors. Therefore, it is important to discuss the applicability of the proposed theoretical model to the experiments at actual conditions.

The comparison of the charging time between the theoretical prediction from τ_{2D} and the experimental evaluation is implemented. For instance, the research[26] on the holey graphene framework constructed a device stack that includes the two electrodes of thickness $H = 140$ μm, separated by an electrolyte layer of thickness $2L = 30$ μm. Observed from the provided HRTEM images of holey graphene sheets, the pore size $\delta = 2$ nm and the distance between adjacent pores $l = 2$ nm are considered. The interlayer spacing of the graphene-based membrane is considered as $h = 1$ nm.[66] An aqueous electrolyte (6 M KOH, bulk diffusivity is considered as $2 \times 10^{-9}\,m^2\,s^{-1}$)[67] and an organic electrolyte (EMIMBF$_4$, bulk diffusivity is considered as $4.29 \times 10^{-11}\,m^2\,s^{-1}$)[68] with the solvent of acetonitrile (AN) at room temperature were used to evaluate the performance of the supercapacitors. It is worth noting that an increase of the screening length at high electrolyte concentration has been identified, a phenomenon that requires a treatment beyond the dilute (Debye−Hückel) regime.[69,70] Therefore, the Debye length calculated by $\lambda_D = \sqrt{\varepsilon k_B T/(2e^2\rho_{bulk})}$ cannot represent the actual screening length at high concentrations and large potentials, making the RC time τ_{RC} obtained from Equation (1) not applicable for the calculation of τ_{2D}. However, a modified relationship was recently found between the RC time at high concentrations and the Debye length λ_D, as given by[60]

$$\tau_{RC} = \frac{2\lambda_D L}{D\left(2 + \frac{\sigma}{\lambda_D}\right)}, \tag{7}$$

with 2 L being the electrode separation and σ being the ion diameter, considering the solvated size of K^+ and OH^- as $\sigma = 0.6$ nm,[71] and the typical size of ionic liquid molecules as $\sigma = 0.5$ nm.[21] The expression for the RC time is obtained from a classical dynamic density functional theory that accounts for electrostatic correlations and for the molecular excluded volume of finite-sized ions and solvent molecules, which is independent on the applied potential.[60] The calculated τ_{RC} for the aqueous electrolyte (6 M KOH) and the organic electrolyte (3 M EMIMBF$_4$/AN) is 0.27 μs and 0.99 μs, respectively. Thus, according to Equation (4), the relaxation timescale τ_{2D} is calculated as 1.4 s (6 M KOH) and 5.3 s (3 M EMIMBF$_4$/AN), respectively, which is indeed of the same order of magnitude as the charging times ~1 s (6 M KOH) and ~ 10 s (EMIMBF$_4$/AN) observed in the experimental data.

The obtained relaxation timescale τ_{2D} is further expected to be used for fitting the experimental cyclic voltammetry (CV) curves. The mathematic expression of the nondimensionless current $j(t)$ in response to an applied periodic potential (Figure 5E) is given in Equation (13) by inserting τ_{2D} into the ECM. In Figure 5F, the nondimensionless CV curves in the experiment[26] for both KOH and EMIMBF$_4$ at different scan rates show similar behaviors (color dots), and we find basic agreement between the experiment and the Equation (13) at the scan frequency $\omega = 0.05\,s^{-1}$ with the fit parameter $\tau_{2D} = 1.4$ s of KOH (red line). Therefore, based on all the discussion above, the influence of the pore structure of the laminated electrode on the charging dynamics can be quite well described by our relatively simple theoretical model.

3 | CONCLUSION

In summary, we studied the charging dynamics in the graphene-based supercapacitors with a representative laminate-electrode model. An ECM and the direct numerical calculations of the PNP equations are combined to quantitively describe the influence of the layered structure on the charging process. Based on the ECM, a simple mathematical expression is proposed to calculate the relaxation timescale (τ_m) that includes the structural contributions of graphene-based electrodes. According to the numerical calculation, for the innermost ($i = 1$) sheet that faces the bulk electrolyte, two relaxation timescales are presented: a generalized RC time τ_{RC} and a diffusion time $L^2/\pi^2 D$. However, for the sheets deeper inside the graphene-based electrode, essentially only the diffusion time is relevant due to the tortuous transport pathways determined by the parameters n and l, which is also the case for practical supercapacitors. Meanwhile, we can obtain the observed relaxation timescale (τ) from the numerical results, providing direct data for us to test the mathematical expression. At low applied potentials with large pore size ($\kappa\delta$) and interlayer spacing (κh), the charging behaviors observed from numerical calculations can be reproduced well by the ECM. Quantitatively, the relaxation timescale τ_m obtained directly from the ECM is modified by a numerical factor upon comparison with the solution of the PNP equations, hence, we obtain $\tau_{2D} = 4\tau_m/\pi^2$, which is applicable for the cases at low electrode potentials without spatial constraints of EDL overlap. The influence of small pore size and interlayer spacing, at which EDLs overlap, as well as high applied potentials on the charging dynamics is further investigated by comparing the corresponding observed relaxation timescales (τ_δ, τ_h, and τ_ϕ) obtained from the numerical results to the τ_{2D}. Inserting parameters relating to an experimental study for the holey graphene frameworks, the proposed formula predicts the relaxation times within the same order of magnitude which is not trivial given the many length- and time scales involved. Meanwhile, with the relaxation timescale τ_{2D} of the laminate-electrode model, our model can reproduce experimental CV curves over a small scan frequency ω. Therefore, our theoretical model can characterize the roles of the structural features of the laminate-electrode model on the charging dynamics, as a general platform to understand the ion transport in two-dimensional materials-based films for compact energy storage. However, more work is needed to establish a closer connection between the laminate-electrode model and experimental features, which should consider the specific surface area of the material, the average pore size, realistic pore morphology, position-dependent diffusion coefficients, etc.

4 | METHODS

4.1 | Equivalent circuit model

The equivalent circuit for the laminate-electrode model in the trivial case $n = 1$ is firstly discussed, as shown in Figure S1, which is consistent with the planar electrode. The EDLs on each electrode are modeled with a capacitor of capacitance C. The electrolyte resistance is

modeled through a resistor of resistance $2R$. Once a potential difference 2Ψ is applied at $t=0$, the capacitor will acquire a time-dependent charge $Q(t)=C\Delta\Psi(t)$, where $\Delta\Psi(t)$ is the time-dependent voltage difference between either side of the capacitors. The current that flows through the system is found via Ohm's law, $I*2R=[\Psi-\Delta\Psi(t)]-[-\Psi+\Delta\Psi(t)]=2[\Psi-\Delta\Psi(t)]$. With $I=\dot{Q}(t)=C\Delta\dot{\Psi}(t)$, we get $\Delta\dot{\Psi}(t)=[\Psi-\Delta\Psi(t)]/RC$. For $\Delta\Psi(t=0)=0$, the $\Delta\Psi(t)$ can be expressed as:

$$\Delta\Psi(t)=\Psi\left[1-\exp\left(-\frac{t}{RC}\right)\right]. \tag{8}$$

Since the EDL capacitance $C=A\varepsilon\kappa$ and electrolyte resistivity $2R=2L/(A\varepsilon\kappa^2D)$ with A the surface area facing the electrolyte and D the ion diffusivity, we can find $RC=\tau_{RC}=\kappa^{-1}L/D$ with τ_{RC} the standard relaxation timescale. The developed relaxation time τ_m for the general n case is discussed in Supplementary Information.

To reproduce cyclic voltammetry (CV) curves with the obtained relaxation timescale, we need to consider the $\Psi(t)$ of a saw-tooth from between zero and a maximum Ψ_0 (Figure 5E), given by:[54,55]

$$\frac{\Psi(t)}{\Psi_0}=\begin{cases}\omega t-2(k-1), & 2(k-1)<\omega t<(2k-1)\\ 2k-\omega t, & (2k-1)<\omega t<2j\end{cases} \tag{9}$$

with $\omega=1/t_0$ the scan rate and $k=1, 2, \ldots$ the cycle number. The Equation (9) can be expanded in Fourier base,

$$\Psi(t)=\Psi_0\left[\frac{1}{2}-\frac{4}{\pi^2}\sum_{m=1,3,5,\ldots}^{\infty}\frac{\cos(m\pi\omega t)}{m^2}\right], \tag{10}$$

and with the initial condition $\Delta\Psi(t)=0$, inserting Equation (10) into the abovementioned equation $\Delta\dot{\Psi}(t)=[\Psi-\Delta\Psi(t)]/\tau_{RC}$ to find

$$\Delta\Psi(t)=\Psi_0\left[\frac{\left(1-e^{-\frac{t}{\tau_{RC}}}\right)}{2}-\frac{4}{\pi^2}\sum_{m=1,3,5,\ldots}^{\infty}\frac{1}{m^2}\frac{\cos(m\pi\omega t)+m\pi\omega\tau_{RC}\sin(m\pi\omega t)-e^{-\frac{t}{\tau_{RC}}}}{1+(m\pi\omega\tau_{RC})^2}\right]. \tag{11}$$

Then, inserting Equation (11) into $I=\dot{Q}(t)=C\Delta\dot{\Psi}(t)$ and using $\nu=\omega t$, we find

$$I(\nu)=\frac{C\Psi_0\omega}{\omega\tau_{RC}}\left[\frac{e^{-\frac{\nu}{\omega\tau_{RC}}}}{2}-\frac{4}{\pi^2}\sum_{m=1,3,5,\ldots}^{\infty}\frac{1}{m^2}\frac{(m\pi\omega\tau_{RC})^2\cos(m\pi\nu)-m\pi\omega\tau_{RC}\sin(m\pi\nu)+e^{-\frac{\nu}{\omega\tau_{RC}}}}{1+(m\pi\omega\tau_{RC})^2}\right]. \tag{12}$$

Moving on to the layered graphene-based electrodes (general n case), we obtain

$$j(\nu)=\frac{1}{\xi}\left[\frac{e^{-\frac{\nu}{\xi}}}{2}-\frac{4}{\pi^2}\sum_{m=1,3,5,\ldots}^{\infty}\frac{1}{m^2}\frac{(m\pi\xi)^2\cos(m\pi\nu)-m\pi\xi\sin(m\pi\nu)+e^{-\frac{\nu}{\xi}}}{1+(m\pi\xi)^2}\right] \tag{13}$$

with the nondimensionless current $j(\nu)=I(\nu)/[(2n-1)C\Psi_0\omega]$ and the non-dimensionless parameter $\xi=\omega\tau_{2D}$. Inserting the relaxation time τ_{2D} into the Equation (13), the equivalent circuit-based CV curve is calculated to fit the experimental CV curve.

4.2 | PNP equations

The PNP equations, which is an effective continuum model, can be solved by the finite element method (FEM) to describe the ionic dynamics in the complex pore structure.[58] The first one (Equation 14) is the continuity Equation and the second one (Equation 15) is Nernst–Planck equation, which signify conservation of mass equation that describes the influence of an ionic concentration gradient and that of an electric field on the flux of ions. The general conservation of mass equation is expressed as:

$$\frac{\partial\rho_{\pm}}{\partial t}+\nabla\cdot\overrightarrow{J_{\pm}}=0, \tag{14}$$

where ρ_i is the number density of anions and cations. Furthermore, the ionic flux $\overrightarrow{J_{\pm}}$ within the solution is given by the following Nernst–Planck equation:

$$\overrightarrow{J_{\pm}}=-D(\nabla\rho_{\pm}\pm\rho_{\pm}\nabla\phi), \tag{15}$$

where the first term is the flux due to diffusion and the second term is the flux due to electro-migration in the electric field, D is the ionic dif-

fusivity, taken to be 1×10^{-9} m^2 s^{-1} for both anion and cation. The ϕ is the dimensionless applied potential of Ψ with respect to the thermal voltage k_BT/e, which satisfies the Poisson equation:

$$\nabla \cdot (-\nabla\phi) = \kappa^2 \left[\frac{\rho_+ - \rho_-}{2\rho_{bulk}}\right]. \quad (16)$$

The above governing equations were solved for specified initial and boundary conditions using the COMSOL Multiphysics finite-element-based solver (https://www.comsol.com/). The simulation domain and mesh setup are shown in Figure S2. The two outermost graphene-based sheets ($i = n$) are impermeable to the electrolyte, such that the system is closed; the initial densities of cations and anions in the electrolyte throughout the cell are homogenous ρ_{bulk} 0.06 nm^{-3} (0.1 M). It is also found that although the diffusion coefficient of ions is considered constant in the structure model when performing the PNP calculations, the structural influence in the apparent ion diffusivity is included through the transfer resistance.

AUTHOR CONTRIBUTIONS

Haolan Tao: Conceptualization (lead); data curation (lead); formal analysis (lead); investigation (equal); methodology (equal); software (equal); validation (equal); visualization (lead); writing – original draft (lead); writing – review and editing (lead). **Zhi Xu:** Funding acquisition (equal); project administration (equal); resources (equal); supervision (equal); validation (equal); writing – review and editing (equal). **Cheng Lian:** Conceptualization (lead); formal analysis (equal); funding acquisition (lead); methodology (equal); project administration (lead); resources (equal); supervision (lead); validation (equal); writing – original draft (equal); writing – review and editing (equal). **Rene van Roij:** Formal analysis (equal); methodology (equal); supervision (equal); writing – original draft (equal); writing – review and editing (equal). **Honglai Liu:** Formal analysis (equal); funding acquisition (equal); project administration (equal); resources (lead); supervision (lead).

ACKNOWLEDGMENTS

This work is sponsored by the National Key R&D Program of China (No. 2019YFC1906702), the National Natural Science Foundation of China (Nos. 91834301, 22078088), and the Shanghai Rising-Star Program (No. 21QA1401900). This work is part of the D-ITP consortium, a program of the Netherlands Organization for Scientific Research (NWO) that is funded by the Dutch Ministry of Education, Culture and Science (OCW). Cheng Lian and René van Roij acknowledge the EU-FET project NANOPHLOW (REP-766972-1). Haolan Tao gratefully acknowledges the financial support from China Scholarship Council.

CONFLICT OF INTEREST STATEMENT

The authors declare no conflict of interest.

DATA AVAILABILITY STATEMENT

The data that support the findings of this study are available from the corresponding author upon reasonable request.

ORCID

Haolan Tao https://orcid.org/0000-0003-4436-9144
Zhi Xu https://orcid.org/0000-0003-2459-0933
Cheng Lian https://orcid.org/0000-0002-9016-832X
René van Roij https://orcid.org/0000-0002-2221-294X
Honglai Liu https://orcid.org/0000-0002-5682-2295

REFERENCES

1. Miller JR. Valuing reversible energy storage. *Science*. 2012;335(6074):1312-1313.
2. Simon P, Gogotsi Y. Materials for electrochemical capacitors. *Nat Mater*. 2008;7(11):845-854.
3. Wang Q, Yan J, Fan Z. Carbon materials for high volumetric performance supercapacitors: design, progress, challenges and opportunities. *Energ Environ Sci*. 2016;9(3):729-762.
4. Simon P, Gogotsi Y. Perspectives for electrochemical capacitors and related devices. *Nat Mater*. 2020;19(11):1151-1163.
5. Burke A. R&D considerations for the performance and application of electrochemical capacitors. *Electrochim Acta*. 2007;53(3):1083-1091.
6. Tao H, Lian C, Liu H. Multiscale modeling of electrolytes in porous electrode: from equilibrium structure to non-equilibrium transport. *Green Energy & Environ*. 2020;5(3):303-321.
7. Zhong C, Deng Y, Hu W, Qiao J, Zhang L, Zhang J. A review of electrolyte materials and compositions for electrochemical supercapacitors. *Chem Soc Rev*. 2015;44(21):7484-7539.
8. Chen M, Wu J, Ye T, et al. Adding salt to expand voltage window of humid ionic liquids. *Nat Commun*. 2020;11(1):5809.
9. Huang J, Sumpter BG, Meunier V. Theoretical model for nanoporous carbon supercapacitors. *Angew Chem Int ed*. 2008;120(3):530-534.
10. Pomerantseva E, Bonaccorso F, Feng X, Cui Y, Gogotsi Y. Energy storage: the future enabled by nanomaterials. *Science*. 2019;366(6468):eaan8285.
11. Zhu Y, Murali S, Stoller MD, et al. Carbon-based supercapacitors produced by activation of graphene. *Science*. 2011;332(6037):1537-1541.
12. Yang X, Cheng C, Wang Y, Qiu L, Li D. Liquid-mediated dense integration of graphene materials for compact capacitive energy storage. *Science*. 2013;341(6145):534-537.
13. El-Kady Maher F, Strong V, Dubin S, Kaner Richard B. Laser scribing of high-performance and flexible graphene-based electrochemical capacitors. *Science*. 2012;335(6074):1326-1330.
14. Li Z, Gadipelli S, Li H, et al. Tuning the interlayer spacing of graphene laminate films for efficient pore utilization towards compact capacitive energy storage. *Nat Energy*. 2020;5(2):160-168.
15. Zhong J, Sun W, Wei Q, Qian X, Cheng HM, Ren W. Efficient and scalable synthesis of highly aligned and compact two-dimensional nanosheet films with record performances. *Nat Commun*. 2018;9(1):3484.
16. Li H, Tao Y, Zheng X, et al. Ultra-thick graphene bulk supercapacitor electrodes for compact energy storage. *Energ Environ Sci*. 2016;9(10):3135-3142.
17. Cheng C, Jiang G, Garvey CJ, et al. Ion transport in complex layered graphene-based membranes with tuneable interlayer spacing. *Sci Adv*. 2016;2(2):e1501272.
18. Nair RR, Wu HA, Jayaram PN, Grigorieva IV, Geim AK. Unimpeded permeation of water through helium-leak-tight graphene-based membranes. *Science*. 2012;335(6067):442-444.
19. Méndez-Morales T, Ganfoud N, Li Z, Haefele M, Rotenberg B, Salanne M. Performance of microporous carbon electrodes for supercapacitors: comparing graphene with disordered materials. *Energy Stor Mater*. 2019;17:88-92.
20. Futamura R, Iiyama T, Takasaki Y, et al. Partial breaking of the coulombic ordering of ionic liquids confined in carbon nanopores. *Nat Mater*. 2017;16(12):1225-1232.

21. Largeot C, Portet C, Chmiola J, Taberna P-L, Gogotsi Y, Simon P. Relation between the ion size and pore size for an electric double-layer capacitor. *J Am Chem Soc*. 2008;130(9):2730-2731.
22. Jiang D-E, Jin Z, Wu J. Oscillation of capacitance inside nanopores. *Nano Lett*. 2011;11(12):5373-5377.
23. Banda H, Daffos B, Périé S, et al. Ion sieving effects in chemically tuned pillared graphene materials for electrochemical capacitors. *Chem Mater*. 2018;30(9):3040-3047.
24. Banda H, Périé S, Daffos B, et al. Sparsely pillared graphene materials for high-performance supercapacitors: improving ion transport and storage capacity. *ACS Nano*. 2019;13(2):1443-1453.
25. Banda H, Périé S, Daffos B, et al. Investigation of ion transport in chemically tuned pillared graphene materials through electrochemical impedance analysis. *Electrochim Acta*. 2019;296:882-890.
26. Xu Y, Lin Z, Zhong X, et al. Holey graphene frameworks for highly efficient capacitive energy storage. *Nat Commun*. 2014;5(1):4554.
27. Liu C, Yan X, Hu F, Gao G, Wu G, Yang X. Toward superior capacitive energy storage: recent advances in pore engineering for dense electrodes. *Adv Mater*. 2018;30(17):1705713.
28. Griffin JM, Forse AC, Tsai W-Y, Taberna P-L, Simon P, Grey CP. In situ NMR and electrochemical quartz crystal microbalance techniques reveal the structure of the electrical double layer in supercapacitors. *Nat Mater*. 2015;14(8):812-819.
29. Forse AC, Merlet C, Griffin JM, Grey CP. New perspectives on the charging mechanisms of supercapacitors. *J Am Chem Soc*. 2016;138(18):5731-5744.
30. Kondrat S, Wu P, Qiao R, Kornyshev AA. Accelerating charging dynamics in subnanometre pores. *Nat Mater*. 2014;13(4):387-393.
31. Noh C, Jung Y. Understanding the charging dynamics of an ionic liquid electric double layer capacitor via molecular dynamics simulations. *Phys Chem Chem Phys*. 2019;21(13):6790-6800.
32. Bi S, Banda H, Chen M, et al. Molecular understanding of charge storage and charging dynamics in supercapacitors with MOF electrodes and ionic liquid electrolytes. *Nat Mater*. 2020;19(5):552-558.
33. Zeng L, Wu T, Ye T, Mo T, Qiao R, Feng G. Modeling galvanostatic charge–discharge of nanoporous supercapacitors. *Nat Comput Sci*. 2021;1(11):725-731.
34. Tao H, Chen G, Lian C, Liu H, Coppens M-O. Multiscale modelling of ion transport in porous electrodes. *AIChE l*. 2022;68(4):e17571.
35. Jiang D-E, Wu J. Microscopic insights into the electrochemical behavior of nonaqueous electrolytes in electric double-layer capacitors. *J Phys Chemi Lett*. 2013;4(8):1260-1267.
36. Jiang J, Cao D, Jiang D-E, Wu J. Kinetic charging inversion in ionic liquid electric double layers. *J Phys Chem Lett*. 2014;5(13):2195-2200.
37. Chmiola J, Yushin G, Gogotsi Y, Portet C, Simon P, Taberna PL. Anomalous increase in carbon capacitance at pore sizes less than 1 nanometer. *Science*. 2006;313(5794):1760-1763.
38. Breitsprecher K, Holm C, Kondrat S. Charge me slowly, I am in a hurry: optimizing charge–discharge cycles in nanoporous supercapacitors. *ACS Nano*. 2018;12(10):9733-9741.
39. Merlet C, Rotenberg B, Madden PA, et al. On the molecular origin of supercapacitance in nanoporous carbon electrodes. *Nat Mater*. 2012;11(4):306-310.
40. Merlet C, Pean C, Rotenberg B, et al. Highly confined ions store charge more efficiently in supercapacitors. *Nat Commun*. 2013;4:2701.
41. Péan C, Merlet C, Rotenberg B, et al. On the dynamics of charging in nanoporous carbon-based supercapacitors. *ACS Nano*. 2014;8(2):1576-1583.
42. Prehal C, Koczwara C, Jäckel N, et al. Quantification of ion confinement and desolvation in nanoporous carbon supercapacitors with modelling and in situ X-ray scattering. *Nat Energy*. 2017;2(3):16215.
43. Forse AC, Griffin JM, Merlet C, et al. Direct observation of ion dynamics in supercapacitor electrodes using in situ diffusion NMR spectroscopy. *Nat. Energy*. 2017;2(3):16216.
44. Liu YM, Merlet C, Smit B. Carbons with regular pore geometry yield fundamental insights into supercapacitor charge storage. *ACS Centr Sci*. 2019;5(11):1813-1823.
45. Li Z, Mendez-Morales T, Salanne M. Computer simulation studies of nanoporous carbon-based electrochemical capacitors. *Curr Opinin Electrochem*. 2018;9:81-86.
46. Cheng C, Jiang G, Simon GP, Liu JZ, Li D. Low-voltage electrostatic modulation of ion diffusion through layered graphene-based nanoporous membranes. *Nat Nanotechnol*. 2018;13(8):685-690.
47. Shim Y, Jung Y, Kim HJ. Graphene-based supercapacitors: a computer simulation study. *J Phys Chem C*. 2011;115(47):23574-23583.
48. Pykal M, Langer M, Blahová Prudilová B, Banáš P, Otyepka M. Ion interactions across graphene in electrolyte aqueous solutions. *J Phys Chem C*. 2019;123(15):9799-9806.
49. Juarez F, Dominguez-Flores F, Quaino P, Santos E, Schmickler W. Interactions of ions across carbon nanotubes. *Phys Chem Chem Phys*. 2020;22(19):10603-10608.
50. Mendez-Morales T, Burbano M, Haefele M, Rotenberg B, Salanne M. Ion-ion correlations across and between electrified graphene layers. *J Chem Phys*. 2018;148(19):193812.
51. Ji H, Zhao X, Qiao Z, et al. Capacitance of carbon-based electrical double-layer capacitors. *Nat Commun*. 2014;5(1):3317.
52. Zhan C, Neal J, Wu J, Jiang D-E. Quantum effects on the capacitance of graphene-based electrodes. *J Phys Chem C*. 2015;119(39):22297-22303.
53. Verkholyak T, Kuzmak A, Kornyshev AA, Kondrat S. Less is more: can low quantum capacitance boost capacitive energy storage? *J Phys Chem Lett*. 2022;13(47):10976-10980.
54. Lian C, Janssen M, Liu H, van Roij R. Blessing and curse: how a supercapacitor's large capacitance causes its slow charging. *Phys Rev Lett*. 2020;124(7):076001.
55. Lin Y, Lian C, Berrueta MU, Liu H, van Roij R. Microscopic model for cyclic voltammetry of porous electrodes. *Phys Rev Lett*. 2022;128(20):206001.
56. Huang P, Tao H, Yang J, Lian C, Liu H. Four stages of thermal effect coupled with ion-charge transports during the charging process of porous electrodes. *AIChE J*. 2022;68:e17790.
57. Janssen M. Transmission line circuit and equation for an electrolyte-filled pore of finite length. *Phys Rev Lett*. 2021;126(13):136002.
58. Bazant MZ, Thornton K, Ajdari A. Diffuse-charge dynamics in electrochemical systems. *Phys Rev E*. 2004;70(2):021506.
59. Janssen M, Bier M. Transient dynamics of electric double-layer capacitors: exact expressions within the Debye-Falkenhagen approximation. *Phys Rev E*. 2018;97(5):052616.
60. Ma K, Janssen M, Lian C, van Roij R. Dynamic density functional theory for the charging of electric double layer capacitors. *J Chem Phys*. 2022;156(8):084101.
61. Ivan Palaia AJA, Patrick B. Warren, Benjamin Rotenberg, Emmanuel Trizac, charging dynamics of electric double layer nanocapacitors in mean-field. *arXiv preprint*. 2023; arXiv:2301.00610.
62. Zhan H, Xiong Z, Cheng C, Liang Q, Liu JZ, Li D. Solvation-involved nanoionics: new opportunities from 2D nanomaterial laminar membranes. *Adv Mater*. 2020;32(18):e1904562.
63. Kavokine N, Netz RR, Bocquet L. Fluids at the nanoscale: from continuum to subcontinuum transport. *Annu Rev Fluid Mech*. 2021;53(1):377-410.
64. Herrero, C, Joly L. *Poisson-Boltzmann formulary*: 2nd ed. *arXiv preprint*. 2022; arXiv:2105.00720.

65. Wang H, Sun X, Liu Z, Lei Z. Creation of nanopores on graphene planes with MgO template for preparing high-performance supercapacitor electrodes. *Nanoscale*. 2014;6(12):6577-6584.
66. Liu G, Jin W, Xu N. Graphene-based membranes. *Chem Soc Rev*. 2015;44(15):5016-5030.
67. Rumble J. *CRC Handbook of Chemistry and Physics*. 100th ed. CRC Press; 2019.
68. Lian C, Zhao S, Liu H, Wu J. Time-dependent density functional theory for the charging kinetics of electric double layer containing room-temperature ionic liquids. *J Chem Phys*. 2016;145(20): 204707.
69. Attard P. Asymptotic analysis of primitive model electrolytes and the electrical double layer. *Phys Rev E*. 1993;48(5):3604-3621.
70. Leote de Carvalho RJF, Evans R. The decay of correlations in ionic fluids. *Mol Phys*. 1994;83(4):619-654.
71. Nightingale ER. Phenomenological theory of ion solvation. Effective radii of hydrated ions. *J Phys Chem*. 1959;63(9):1381-1387.

SUPPORTING INFORMATION

Additional supporting information can be found online in the Supporting Information section at the end of this article.

How to cite this article: Tao H, Xu Z, Lian C, van Roij R, Liu H. Charging dynamics in a laminate-electrode model for graphene-based supercapacitors. *AIChE J*. 2023;69(10): e18189. doi:10.1002/aic.18189